

Evaluation of aluminum critical point using an *ab initio* variational approach

Gérald Faussurier,^{1,*} Christophe Blancard,¹ and Pier Luigi Silvestrelli²

¹CEA, DAM, DIF, F-91297 Arpajon, France

²Dipartimento di Fisica “G. Galilei,” Università di Padova, via Marzolo 8, I-35131 Padova, Italy
and DEMOCRITOS National Simulation Center, 34014 Trieste, Italy

(Received 12 December 2008; published 3 April 2009)

We present a method to evaluate the critical point of aluminum using a variational approach based on the *ab initio* molecular-dynamics code CPMD. We found that the critical density, temperature, and pressure are equal to 0.44 g/cm³, 7963 K, and 0.35 GPa, respectively. At the critical point, the system is rarefied, coupled, and degenerate. The shear-viscosity and the self-diffusion were estimated at the critical point. Using the Kubo-Greenwood formula, we obtained the electrical conductivity, the absorption coefficient, the index of refraction, and the reflectivity at the critical point. We followed Mott’s ideas to study the metal-nonmetal transition related to the critical point. Our method can be useful to investigate phase transition and the critical point of metals.

DOI: 10.1103/PhysRevB.79.134202

PACS number(s): 05.70.Jk, 05.70.Ce, 71.15.Pd

I. INTRODUCTION

Warm dense matter (WDM) is a form of strongly coupled high energy density matter intermediate between condensed matter and plasmas. These high-density (~ 0.1 to 10 g/cm³) and moderate-temperature (~ 1 eV) states of matter are very difficult to study analytically or by numerical simulations. They prove to be challenging and fascinating to investigate experimentally^{1–15} and are of key interest in astrophysics or inertial fusion science.¹⁶

As far as metals are concerned, the liquid state covering the temperature range from the melting point to the critical temperature, which, for some metals, can exceed 10 000 K, is excessively difficult to study experimentally and theoretically.^{17–19} This challenging regime is closely related to the metal-nonmetal transition.^{20,21} The description of critical point region from first principles is complicated. Using the *ab initio* molecular-dynamics code CPMD,^{22–24} we propose a scheme based on a variational approach²⁵ to investigate the region close to the critical point of metals. This method is applied to the evaluation of the critical point of aluminum.

This paper is organized as follows. In Sec. II, we present the method utilized to evaluate the critical point of aluminum. In Sec. III, we present results concerning the aluminum critical point, transport coefficients, but also various spectral quantities that can be derived from the Kubo-Greenwood formula, such as absorption coefficient, index of refraction, or reflectivity. We discuss the metal-nonmetal transition with respect to Mott’s ideas. Sec. IV is the conclusion.

II. METHOD

Assuming that we could describe atoms in disordered matter with a hard-sphere reference system, we placed N_a nuclei inside a cubic supercell with periodic boundary conditions at given hard-sphere packing fraction η using Monte Carlo simulations. This was performed for a single element in thermodynamic equilibrium at given mass density ρ and temperature T . For such an ionic configuration, we calculated the electronic free energy F_e and the electrostatic

ionic energy U_{II} with the CPMD code.²⁶ We used a very good analytic expression for the excess ionic entropy per ion $s_{\text{exc}}^{\text{HS}} = -\frac{\eta(4-3\eta)}{(1-\eta)^2}$. This semiempirical expression is known to match molecular-dynamics simulations up to the hard-sphere melting conditions.²⁷ We selected N_c statistically independent ionic configurations at given η . We then calculated the average $\langle F_e + U_{II} \rangle$ over the N_c configurations of $(F_e + U_{II})$ to obtain the reduced excess free energy f_{exc} of the electron and ion system,

$$f_{\text{exc}} = \beta \langle F_e + U_{II} \rangle / N_a - s_{\text{exc}}^{\text{HS}}, \quad (1)$$

where $\beta = 1/(k_B T)$. k_B is the Boltzmann constant. It can be shown that f_{exc} is an upper bound of the exact reduced excess free energy of the electron and ion system.²⁵ The effective hard-sphere packing fraction η_{eff} was found by minimizing the right-hand side of Eq. (1). For the thermodynamic conditions encountered in this work, it has been found sufficient to determine η_{eff} with an accuracy of 0.01. Adding to f_{exc} in Eq. (1) the reduced free energy f_0 of the ideal gas,²⁸ we obtained the best total reduced free energy $f = f_0 + f_{\text{exc}}$ of the electron and ion system in the sense of the Gibbs-Bogolyubov inequality.²⁵ From f , we could derive in a self-consistent way the equation of state of the material.

This method known as HS-AIMD for hard-sphere *ab initio* molecular dynamics²⁵ is faster than usual quantum molecular-dynamics simulations since no dynamics simulations are performed with the *ab initio* molecular-dynamics code. The HS-AIMD is a logical follow-on to the work developed in the context of liquid metal^{29,30} and later adapted and extended in the plasma physics field.^{31,32} The HS-AIMD scheme has been compared successfully to quantum molecular-dynamics simulations and to experimental results²⁵ for expanded Al.

The HS-AIMD method is well suited to describe thermodynamical properties of expanded material for temperature above the melting temperature. As an illustration, we have chosen to evaluate the critical point of aluminum. We have performed HS-AIMD calculations for ρ between 0.1 and 1.4 g/cm³ and T between 6000 and 9000 K. Initially, we were looking for a critical density around 0.7–0.8 g/cm³

and a critical temperature between 6000 and 8000 K.³³ We used $N_a=32$ and $N_c=30$. The interaction between ions and valence electrons has been modeled using a norm-conserving pseudopotential with s and p nonlocalities.³⁴ The electronic orbitals were expanded in plane waves with a cutoff of 16 Ry. This aluminum pseudopotential has been carefully tested and successfully used in quantum molecular dynamics (QMD) simulations of solid and molten aluminum at the melting point³⁵ and to study metal-insulator transition in dense aluminum.²⁶ Since the CPMD code has been used successfully for aluminum from liquid-metal conditions to expanded regime,^{25,26,33} we have kept the same CPMD parameters to consider the region close to the aluminum critical point to calculate F_e in Eq. (1) and to determine the effective hard-sphere packing-fraction η_{eff} . For densities between 0.7 and 1.4 g/cm³ we used 320 electronic states, for $\rho=0.6$ and 0.7 g/cm³ 400 electronic states, for $\rho=0.4$ g/cm³ 600 electronic states, for $\rho=0.3$ g/cm³ 800 electronic states, for $\rho=0.2$ g/cm³ 1000 electronic states, and for $\rho=0.1$ g/cm³ 1200 electronic states. In density, calculations were done every 0.1 g/cm³ between 0.1 and 1.4 g/cm³. In temperature, calculations were first performed for $T=6000, 7000, 8000$, and 9000 K, i.e., for a rough mesh in temperature. At fixed temperature, we have fitted the reduced excess free energy f_{exc} in Eq. (1) by a cubic polynomial in density. At fixed density, we have used a cubic spline interpolation³⁶ in temperature of the coefficients of the cubic polynomial in density. This allowed us to estimate f_{exc} anywhere in the density-temperature plane with $0.1 \leq \rho \leq 1.4$ g/cm³ and $6000 \leq T \leq 9000$ K. From f_{exc} we had access to pressure P and to its first $\frac{\partial P}{\partial \rho}|_T$ and second $\frac{\partial^2 P}{\partial \rho^2}|_T$ derivatives with respect to density. We have then searched by iterations the isotherm $\rho \rightarrow P(\rho, T)$ that had an inflexion point with a tangent parallel to the density axis. The density ρ_c and temperature T_c for which we had simultaneously $\frac{\partial P}{\partial \rho}|_T(\rho_c)=0$ and $\frac{\partial^2 P}{\partial \rho^2}|_T(\rho_c)=0$ determined the critical point. From the equation of state $P(\rho, T)$ we have obtained the pressure at the critical point. With the initial mesh in temperature, the critical temperature was found to be close to 8000 K. We then launched calculations for temperatures equal to 7200, 7400, 7600, 7800, 8200, 8400, 8600, and 8800 K. This represents a total of 168 (ρ, T) points in the density-temperature plane. The Γ point was used to sample the Brillouin zone of the supercell to obtain these 168 (ρ, T) points.

III. RESULTS AND DISCUSSION

In the present situation, we have found for aluminum $\rho_c = 0.44$ g/cm³, $T_c = 7963$ K, and $P_c = 0.35$ GPa. We plot in Fig. 1 the critical curve obtained with the HS-AIMD approach with two other isotherms, one above T_c ($T=9000$ K) and one below T_c ($T=7000$ K). We have used the Maxwell construction^{37,38} to obtain the isotherm $T=7000$ K. We have extrapolated to zero density the various isotherms using a cubic interpolation between 0 and 0.1 g/cm³. We have used the values of P , $\frac{\partial P}{\partial \rho}$ and $\frac{\partial^2 P}{\partial \rho^2}$ at $\rho=0.1$ g/cm³ to do so. This extrapolation has only been used to produced Fig. 1 since we needed values of pressure below 0.1 g/cm³ for the Maxwell

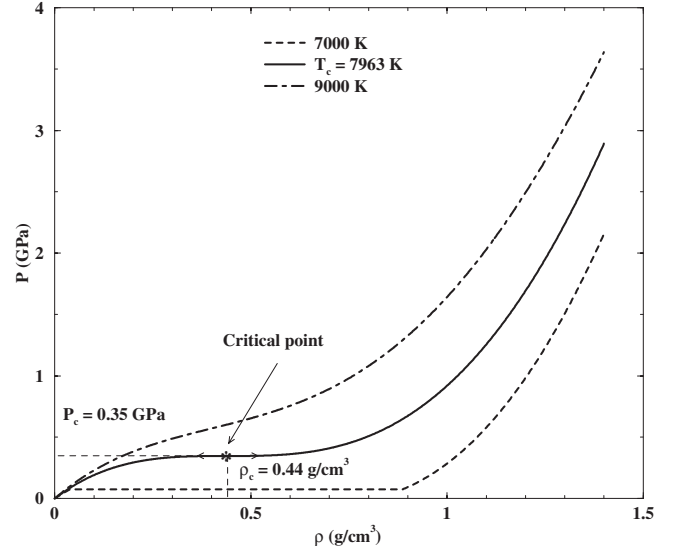


FIG. 1. Critical curve of aluminum obtained with the HS-AIMD approach. The critical point is located at $\rho_c=0.44$ g/cm³ and $T_c=7963$ K for which $P_c=0.35$ GPa. Two isotherms below and above T_c are also shown.

construction. The critical density is a little bit lower than what we initially expected. The critical temperature is very close to the upper bound of the expected initial interval, i.e., 8000 K. In Table I we compare our results with other theoretical calculations. The critical compressibility factor $Z_c = \frac{AP_c}{\mathcal{N}\rho_c k_B T_c}$, where A and \mathcal{N} are the molar mass of the element and the Avogadro number, respectively. The critical compressibility factor found in Table I is always lower than one. This means that the thermodynamic conditions in the vicinity of the critical point are not those of an ideal gas. We can see that there are large discrepancies between various calculations. There are nearly a factor 3, 1.5, and 3 between the extreme values of ρ_c , T_c , and P_c , respectively. If we calculate the averages and the standard deviations corresponding to the values presented in Table I, we found 7620 and 1190 K for the critical temperature, 0.52 and 0.19 g/cm³ for the critical density, and 0.39 and 0.14 GPa for the critical pressure, respectively. The values found with the HS-AIMD ap-

TABLE I. Critical density ρ_c , temperature T_c , and pressure P_c of aluminum obtained by Young and Alder (Ref. 43), Likalter (Ref. 44), Hess (Ref. 45), Singh *et al.* (Ref. 46), Ray *et al.* (Ref. 47), Lomonosov (Ref. 48), and the HS-AIMD approach. ρ_c is in g/cm³, T_c in kelvin, and P_c in GPa. Z_c is the critical compressibility factor.

	ρ_c	T_c	P_c	Z_c
Young and Alder (Ref. 43)	0.69	7151	0.5458	0.36
Likalter (Ref. 44)	0.28	8860	0.468	0.61
Hess (Ref. 45)	0.43	8944	0.4726	0.40
Singh <i>et al.</i> (Ref. 46)	0.785	8472	0.5094	0.25
Ray <i>et al.</i> (Ref. 47)	0.32	5700	0.187	0.33
Lomonosov (Ref. 48)	0.703	6250	0.197	0.15
HS-AIMD	0.44	7963	0.35	0.32

proach are quite close to these average values. Results presented in Table I indicate that any measurement with an uncertainty lower than 20% is already sufficient to discriminate between the theoretical approaches.^{43–46,48}

The aluminum critical point has been estimated using full QMD simulations by Desjarlais. Critical parameters ρ_c , T_c , and P_c estimated by Desjarlais are close to Lomonosov⁴⁸ calculations. They are different from our results. Desjarlais' calculations indicate a critical temperature of 6250 K and a critical pressure close to 0.2 GPa. It is said in Ref. 48 that “the density of the critical point is also very close to the QMD result.” If we look carefully at Fig. 14 of Ref. 48, we can see that the QMD isotherm at 6250 K is flat between 0.5 and 0.7 g/cm³. This illustrates the fact that it is difficult to estimate the critical density with full QMD simulations. What is surprising is the fact that full QMD simulations predict an aluminum critical temperature of 6250 K whereas HS-AIMD simulations give 7963 K. There is a difference of 1713 K between the full QMD and HS-AIMD simulations. The difference in pressure is also noticeable since the relative error between the two calculations nearly reaches 50%. There are many causes that could explain these differences, i.e., the QMD codes, the role of higher points sets for evaluating the Brillouin zone, the use of hard-sphere reference system, or the thermodynamic limit. The explanation of this discrepancy deserves a particular study. We know that the thermodynamic limit is very important to describe the critical point domain.^{39,40} Using periodic boundary conditions is an artificial way to mimic the thermodynamic limit. This means that one has to check how results depend on N_a and to try to find the results at the thermodynamic limit.^{41,42} However, at present it is not possible to study how the critical pressure, density, and temperature change with N_a , to determine their thermodynamic values, and to compare HS-AIMD calculations with full QMD simulations if no breakthrough occurs to increase the efficiency of the numerics.

We plot in Fig. 2 the effective hard-sphere packing fraction η_{eff} found with the HS-AIMD approach as a function of density for all the temperatures inside the density-temperature plane selected to determine the critical point. We see that η_{eff} is nearly linear with density and depends very little on temperature. A simple linear regression shows that

$$\eta_{\text{eff}} = 0.3\rho/\rho_0 \quad (2)$$

inside the present density-temperature plane, where $\rho_0 = 2.7 \text{ g/cm}^3$ is the aluminum solid density. In Eq. (2), ρ is in g/cm³. We thus find that the hard-sphere packing fraction η_c at the critical point is close to 0.05. This result for η_c is lower than the one predicted by Young and Alder,⁴³ i.e., 0.130 44. In any case, the hard-sphere reference system is rather rarefied at the critical point. This does not mean of course that the system is close to an ideal rarefied gas. There is a complex role played by the three-dimensional (3D) coupling between electronic and ionic structures, not to mention the exchange and correlation effects. If we use the correspondence between the one-component plasma and the hard-sphere systems based on the Gibbs-Bogolyubov inequality,³¹ we find that an effective hard-sphere packing-fraction close to 0.05 corresponds to an effective plasma coupling parameter Γ_{eff}

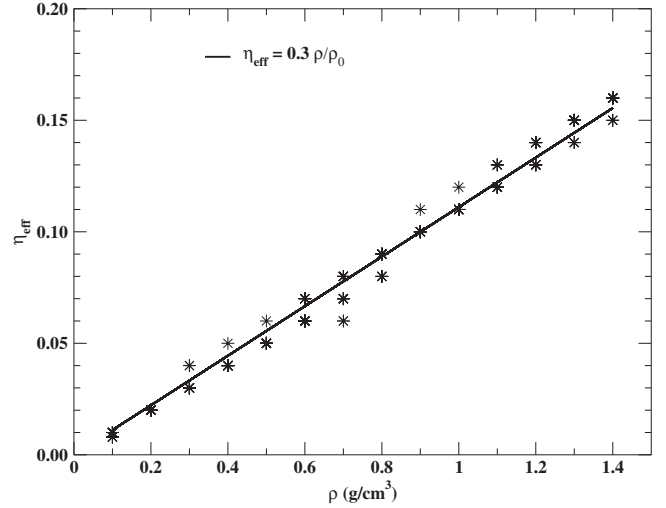


FIG. 2. Effective hard-sphere packing fraction η_{eff} found with the HS-AIMD approach as a function of density ρ for all the temperatures inside the density-temperature plane selected to determine the critical point. We plot the linear regression curve of the data $\eta_{\text{eff}} = 0.3\rho/\rho_0$, where $\rho_0 = 2.7 \text{ g/cm}^3$ is the aluminum solid density.

close to one. At the critical point, the plasmalike system is coupled.

Once determined the critical density and temperature, we can estimate transport coefficients using the transport coefficients of the effective hard-sphere reference system²⁵ at the effective hard-sphere packing-fraction $\eta_c = 0.05$. As an illustration, we found for self-diffusion and shear viscosity 68.30 Å²/ps and 0.31 GPa ps, respectively. The values should be compared to what can be estimated at melting conditions ($\rho = 2.37 \text{ g/cm}^3$ and $T = 933 \text{ K}$), i.e., 0.77 Å²/ps and 1.14 GPa ps, respectively. If the shear viscosity at the critical point is nearly four times lower than the one at melting, there is a huge difference between the self-diffusion coefficient values at melting and at the critical point. Using the Stokes-Einstein relation with slip boundary condition²⁸ to determine the shear viscosity from the self-diffusion coefficient, we found that the shear viscosity at the critical point is equal to 0.12 GPa ps, compared to 0.31 GPa ps. The thermodynamic conditions at the critical point are far from being those for which the Stokes-Einstein relation with slip boundary condition is valid. The situation with the Stokes-Einstein relation with stick boundary conditions²⁸ is worse.

Using the Kubo-Greenwood formula,^{26,33} we can calculate the ac and dc electronic electrical conductivities at the critical point. Many properties follow directly from the knowledge of the frequency-dependent real part of the conductivity.⁴⁹ Calculations have been performed with a 8 k point sampling of the Brillouin zone according to the prescription of Monkhorst and Pack.⁵⁰ Using a cubic fit of the ac electrical conductivity between 0.1 and 0.9 eV and extrapolating to zero frequency the fit, we found a dc electrical conductivity equal to $1.056 \times 10^5 \Omega^{-1} \text{ m}^{-1}$. This gives us an electrical resistivity equal to 9.47 μΩ m. This value is consistent with the measurements obtained by Korobenko *et al.*⁷ at 0.5 g/cm³ and between 6000 and 10 000 K. For instance, at 0.5 g/cm³ and 8446 K, Korobenko *et al.*⁷ measured an

electrical resistivity equal to $11.49 \mu\Omega \text{ m}$. At melting, i.e., for $\rho=2.37 \text{ g/cm}^3$ and $T=933 \text{ K}$, the experimental electrical resistivity is equal to $0.242 \mu\Omega \text{ m}$.²⁹ There is a factor around 40 between the values at the critical point and at melting.

It is well known that the critical point of metals cannot be analyzed without considering its relation to the metal-nonmetal transition.²⁰ Following Hess *et al.*¹⁸ and the inspection of the ac electronic electrical conductivity as a function of frequency, one can say that the system still presents a plasmlike character at the critical point although it really becomes difficult to assume a Drude law at low frequency. To characterize the metal-nonmetal transition, we can use Mott's ideas.

Mott proposed^{51,52} that the metal-nonmetal transition occurred when

$$N_e^{1/3} \kappa \frac{\hbar^2}{m_e e^2} \approx 0.2, \quad (3)$$

where N_e is the electron density, κ the static relative permittivity, \hbar the reduced Planck constant, m_e the electron mass, and e the elementary charge. In literature, we can find^{53,54} 0.25 instead of 0.2. Equation (3) is understood to be a useful way to localize the metal-nonmetal transition. κ can be obtained from the ac electronic electrical conductivities using Kramers-Kronig relations.⁴⁹ At the critical point, we found that $\kappa=12.37$. The problem is now to determine N_e . We can write $N_e=\rho Z_{\text{eff}}\mathcal{N}/A$, where Z_{eff} is the effective number of free electrons per atom. We cannot estimate the number Z_{eff} of atomiclike free electrons per atom from the electrical conductivity using the Kubo-Greenwood formula since we do not have any Drude-type behavior at low frequency. Indeed, there are many possibilities to estimate Z_{eff} . We can simply take $Z_{\text{eff}}=3$. We can deduce Z_{eff} from the effective plasma coupling parameter $\Gamma_{\text{eff}}\approx 1$. Taking $T=7963 \text{ K}$ and $\rho=0.44 \text{ g/cm}^3$, we find that $Z_{\text{eff}}=0.37$. We can also estimate Z_{eff} from the marked minimum in the index of refraction⁵⁵ which corresponds to the plasma frequency at this density. We plot in Fig. 3 the index of refraction as a function of photon energy. The minimum is close to 7.13 eV. From the plasma frequency formula,

$$\omega_p = \sqrt{4\pi e^2 Z_{\text{eff}} N_i / m_e}, \quad (4)$$

where $N_i=\rho\mathcal{N}/A$ is the ion density, we find that $Z_{\text{eff}}=3.75$. The three evaluations of Z_{eff} are quite different. They correspond to three different methods to estimate Z_{eff} in an *ab initio* code. In any case, we find that the left-hand side of Eq. (3) is greater than 0.2 or 0.25. Following Mott and Eq. (3), we are metallic at the critical point. One can note that Mott criterion (3) should be used with caution in *ab initio* codes. This is due to the fact that we have many possibilities to estimate the electron density N_e appearing in Eq. (3). Moreover, Eq. (3) appears sometimes with m_e replaced by an effective mass m_{eff} .⁵⁶

There is another possibility to study the metal-nonmetal transition. It is based on the concept of minimum conductivity enhanced by Mott.^{52,57,58} When the scattering becomes

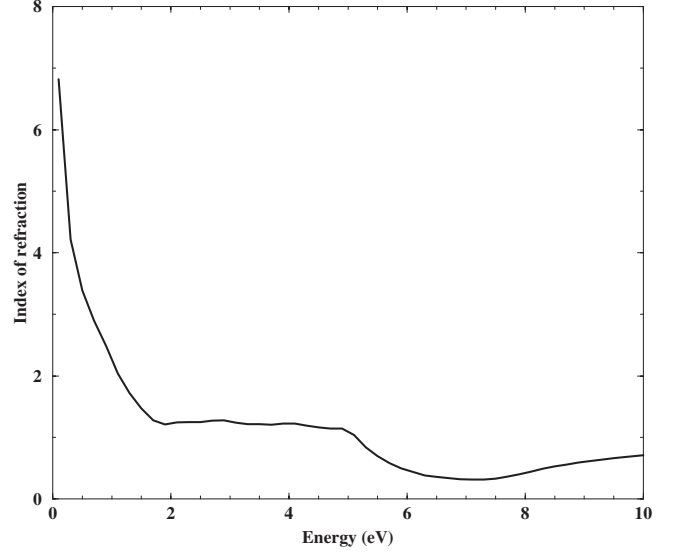


FIG. 3. Aluminum index of refraction at the critical point $\rho_c=0.44 \text{ g/cm}^3$ and $T_c=7963 \text{ K}$.

strong enough for the mean free path to be comparable with the interatomic distance,^{7,11,58–60} the smallest conductivity we can have is^{52,57}

$$\sigma_{\text{min}} \sim \frac{e^2}{3\hbar a}. \quad (5)$$

When the conductivity is above this value, we are in a metallic state. When it is below, we have an insulator.⁶¹ Equation (5) can be helpful to analyze a metal-nonmetal transition. Using Eq. (2), we can estimate the average nearest-neighbor interatomic distance a appearing in Eq. (5) using the nearest-neighbor distribution functions and their related quantities for the hard-sphere system.^{62,63} By means of the Carnahan-Starling approximation,²⁷ we find⁶³

$$a = 2a_{\text{WS}} \eta_{\text{eff}}^{1/3} \left[1 + \int_1^\infty E_P(x) dx \right], \quad (6)$$

where $a_{\text{WS}}=(4\pi N_i/3)^{-1/3}$ is the Wigner-Seitz radius,

$$E_P(x) = \exp\{-\eta_{\text{eff}}[8e(\eta_{\text{eff}})(x^3-1) + 12f(\eta_{\text{eff}})(x^2-1) + 24g(\eta_{\text{eff}})(x-1)]\} \quad (7)$$

for $x \geq 1$ with

$$e(\eta_{\text{eff}}) = \frac{1 + \eta_{\text{eff}}}{(1 - \eta_{\text{eff}})^3}, \quad (8)$$

$$f(\eta_{\text{eff}}) = \frac{-\eta_{\text{eff}}(3 + \eta_{\text{eff}})}{2(1 - \eta_{\text{eff}})^3}, \quad (9)$$

$$g(\eta_{\text{eff}}) = \frac{\eta_{\text{eff}}^2}{2(1 - \eta_{\text{eff}})^3}. \quad (10)$$

At $\rho=0.44 \text{ g/cm}^3$, we find that $\rho_{\text{min}}=1/\sigma_{\text{min}}=3.39 \mu\Omega \text{ m}$ that should be compared to $9.47 \mu\Omega \text{ m}$. This means that we are insulator at the critical density using the minimum con-

ductivity idea based on Eq. (5). From Ref. 64, we can assume that the dc conductivity scales as $\rho^{7/3}$. We can thus estimate the metal-nonmetal density ρ_{mnm} when σ_{min} in Eq. (5) is equal to the DC conductivity using the scaling and the value of $9.47 \mu\Omega \text{ m}$ at $\rho=0.44 \text{ g/cm}^3$. We find $\rho_{\text{mnm}}=0.686 \text{ g/cm}^3$. If these calculations are correct and if aluminum is metallic at the critical density, the critical density may be rather close to 0.7 g/cm^3 . This seems to indicate that we underestimate the critical density using HS-AIMD.

We clearly need experimental data to cross-check these results. We can use experimental data obtained by Korobenko *et al.*^{7,11} They found a change of slope for the electrical resistivity with temperature as we go from 1.4 to 0.1 g/cm^3 . This change of slope was associated with a metal-nonmetal transition.¹¹ Using the data^{7,65} of electrical resistivity as a function of temperature for $\rho=0.1, 0.3, 0.5, 0.675, 1,$ and 1.4 g/cm^3 , we can fit them with a linear regression and obtain the slope as a function of density. This slope is negative at low density and positive at high density. Using cubic interpolation, we find that the slope is zero at $\rho=0.73 \text{ g/cm}^3$, i.e., between 0.675 and 1 g/cm^3 . If aluminum is metallic at the critical point and if the metal-nonmetal is mostly driven by density, this means that the aluminum critical density should be greater than 0.73 g/cm^3 . Indeed, if we plot the logarithm of the resistivity as a function of $1/T^{1/4}$ for the data of Korobenko *et al.*,⁷ we find a characteristic behavior similar to Fig. 5 of Mott,⁵⁷ indicating again a metal/insulator transition lying somewhere between 0.675 and 1 g/cm^3 . If we consider the new data of Korobenko *et al.*¹¹ that are better than the old ones,^{11,65} the resistivity slope changes with its sign at a density that is about three times less than the standard solid density, i.e., 0.9 g/cm^3 . Indeed, the derivative turns to zero somewhere between 0.9 and 1 g/cm^3 , but most likely⁶⁵ closer to 1 g/cm^3 . If this behavior is the onset of a metal-nonmetal transition and if aluminum is metallic at the critical point, the new data¹¹ tend to indicate that there is no theoretical approach presented in Table I that predicts a critical density between 0.9 and 1 g/cm^3 .

Using the index of refraction to estimate the plasma frequency was underlined by Mazevet *et al.*⁵⁵ These authors present various index of refraction at $T=10\,000 \text{ K}$ of aluminum for $\rho=0.025, 0.1, 0.3, 0.5, 1,$ and 2 g/cm^3 in Fig. 5 of Ref. 55. Our results presented in Fig. 3 are consistent with their results shown in Fig. 5 of Ref. 55, though our plateau between 2 and 4 eV is more pronounced. What is interesting is to extract Z_{eff} from the marked minimum associated with plasma frequency. Using Eq. (4), the plasma frequency at 2 g/cm^3 corresponding to an ionization fraction $Z_{\text{eff}}=3$ is 13.52 eV , i.e., in fair agreement with the minimum of the index of refraction shown in Fig. 5 of Ref. 55. This is what is expected from cold dense aluminum. From Fig. 5 of Ref. 55, the minima at $1, 0.5,$ and 0.3 g/cm^3 are close to $9, 7.25,$ and 6.5 eV , respectively. With $Z_{\text{eff}}=3$, the plasma frequencies are $9.61, 6.79,$ and 5.26 eV , respectively. There are some differences. If we use the energies corresponding to the minima and Eq. (4), we find that $Z_{\text{eff}}=2.63, 3.42,$ and 4.58 at $1, 0.5,$ and 0.3 g/cm^3 , respectively. We are below 3 at 1 g/cm^3 but clearly above 3 at 0.3 and 0.5 g/cm^3 . Combining Eq. (4) and the energy minima can lead to questionable results concern-

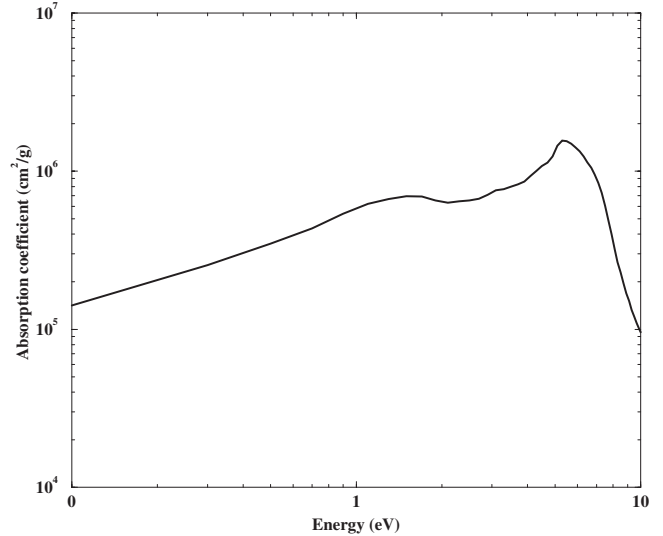


FIG. 4. Aluminum mass absorption coefficient at the critical point $\rho_c=0.44 \text{ g/cm}^3$ and $T_c=7963 \text{ K}$.

ing the effective number of free electrons per atom Z_{eff} when the ac electrical conductivity is not Drude type.^{33,64} Not surprisingly, if we use $Z_{\text{eff}}=3.75$ at $T=7963 \text{ K}$ and $\rho=0.44 \text{ g/cm}^3$, we find an effective plasma coupling parameter of 102 that is very different from $\Gamma_{\text{eff}} \approx 1$. The value of 102 is consistent with what can be extracted from Fig. 5 of Ref. 55. $\eta_c \approx 0.05$ is found with the HS-AIMD approach based on the Gibbs-Bogolyubov inequality using the CPMD code.²⁵ We then used a correspondence between the one-component plasma and the hard-sphere systems using again the Gibbs-Bogolyubov inequality³¹ to get $\Gamma_{\text{eff}} \approx 1$. This value for Γ_{eff} derives from a clear thermodynamic approach. The value 102 comes from a less firm theoretical basis.

Knowing the electron density, one can estimate the degree of degeneracy of the thermodynamic system at the critical point. From $Z_{\text{eff}}=0.37$ we find a degeneracy factor $\Theta=T/T_F=0.80$ where T_F is the Fermi temperature.²⁸ If we use $Z_{\text{eff}}=3$ and $Z_{\text{eff}}=3.75$, we find that $\Theta=0.20$ and $\Theta=0.17$, respectively. In any case, the system at the critical point is degenerate.

We plot in Fig. 4 the mass absorption coefficient at the critical point conditions as a function of photon energy. We see a prominent feature below located around 5.5 eV . This feature is characteristic of the $3s \rightarrow 3p$ transition for an isolated aluminum atom,⁶⁴ which is also present in the metal-nonmetal transition of aluminum at $10\,000 \text{ K}$.³³ If we take $Z_{\text{eff}}=3$ electrons per atom as atomlike free electrons, we find a plasma frequency equal to 6.4 eV . However, in this range of temperature and density, there is a significant number of atomlike electrons that cannot be considered as free but rather localized, as shown by the characteristic feature located around 5.5 eV . From the marked minimum in the index of refraction, one obtained a plasma frequency close to 7.13 eV . However, if we take $Z_{\text{eff}}=0.37$, we obtain a plasma frequency equal to 2.24 eV . Aluminum atoms near the critical point are nearly neutral but the plasma frequency deduced from the index of refraction is not very far from the one obtained using $Z_{\text{eff}}=3$. The plasma frequency is signifi-

cantly reduced from the former estimations if we take $Z_{\text{eff}}=0.37$. This underlines that standard textbook formulas should be used with caution in such a complicated thermodynamic regime. The characteristic feature of the $3s \rightarrow 3p$ transition for an isolated aluminum atom, which is estimated to be below the plasma frequency if we use $Z_{\text{eff}}=3$ or the index of refraction, appears to be above the plasma frequency derived using $Z_{\text{eff}}=0.37$ and Eq. (4). This is very important from an experimental point of view if we want to measure this characteristic feature around 5.5 eV.

We know that the Rosseland weighting factor has a maximum at four times the temperature, i.e., the domain of photon energies that brings a significant contribution in the energy transfer process.⁶⁶ At the critical point, we find that the Rosseland weighting factor is maximum at 2.74 eV. This Rosseland weighting factor is close to the characteristic feature of the $3s \rightarrow 3p$ transition for an isolated aluminum atom. The maximum Rosseland weighting factor is above the plasma frequency obtained using $Z_{\text{eff}}=0.37$ but below both the ones obtained using either $Z_{\text{eff}}=3$ or the index of refraction.

We plot in Fig. 5 the reflectivity at the critical conditions as a function of photon energy. We see that the reflectivity drops rapidly at low frequencies. The reflectivity goes through a minimum between 2 and 4 eV, while the index of refraction is constant in Fig. 3 in this spectral range. Whereas the index of refraction then shows a marked minimum near 7.13 eV before increasing again to tend to one, the reflectivity shows a marked maximum close to both the marked minimum of the index of refraction in Fig. 3 and the characteristic of the $3s \rightarrow 3p$ transition for an isolated aluminum atom visible on the mass absorption coefficient in Fig. 4 in this spectral region.

IV. CONCLUSION

We have evaluated the critical point of aluminum using the variational approach HS-AIMD based on the *ab initio* molecular-dynamics code CPMD. We found that the critical density, temperature, and pressure are equal to 0.44 g/cm³, 7963 K, and 0.35 GPa, respectively. At the critical point, the

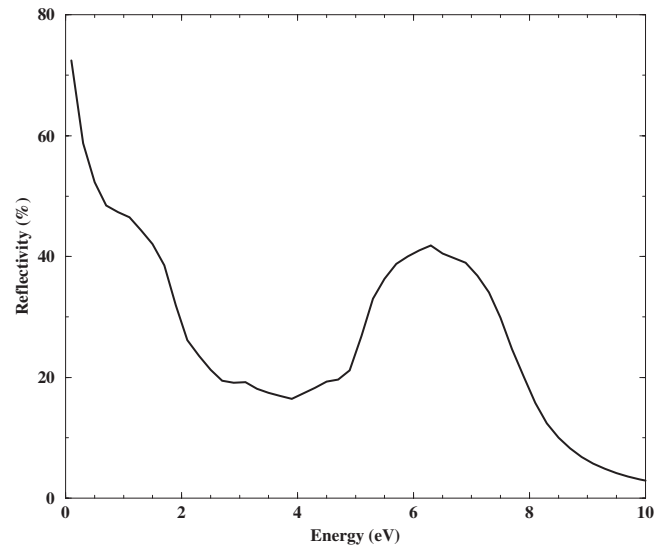


FIG. 5. Aluminum reflectivity at the critical point $\rho_c=0.44$ g/cm³ and $T_c=7963$ K.

system is rarefied, coupled, and degenerate. Using the Kubo-Greenwood formula, we obtained the electrical conductivity, the absorption coefficient, the refraction index, and the reflectivity at the critical point. We used Mott's ideas to study the metal-nonmetal transition, which is strongly related to the critical point. The critical point of aluminum is challenging from a theoretical and an experimental point of view, although it is not easy to analyze it in an unambiguous way. This clearly illustrates the fact that it is difficult to describe a WDM state, such as the aluminum critical point, from a solid-state physics or a plasma physics perspective. This is characteristic of the WDM regime, and this should motivate experimentalists to measure data inside the WDM regime near the critical point of metals.

ACKNOWLEDGMENTS

We thank helpful discussions with M. Desjarlais and S. Libby.

*Corresponding author; gerald.faussurier@cea.fr

¹A. W. DeSilva and J. D. Katsouras, Phys. Rev. E **57**, 5945 (1998).

²I. Krisch and H. J. Kunze, Phys. Rev. E **58**, 6557 (1998).

³J. F. Benage, W. R. Shanahan, and M. S. Murillo, Phys. Rev. Lett. **83**, 2953 (1999).

⁴J. F. Benage, Phys. Plasmas **7**, 2040 (2000).

⁵P. Renaudin, C. Blancard, G. Faussurier, and P. Noiret, Phys. Rev. Lett. **88**, 215001 (2002).

⁶P. Renaudin, C. Blancard, J. Cl rouin, G. Faussurier, P. Noiret, and V. Recoules, Phys. Rev. Lett. **91**, 075002 (2003).

⁷V. N. Korobenko, A. D. Rakhel, A. I. Savvatimski, and V. E. Fortov, Phys. Rev. B **71**, 014208 (2005).

⁸J. Cl rouin, P. Renaudin, Y. Laudernet, P. Noiret, and M. P. Des-

jarlais, Phys. Rev. B **71**, 064203 (2005).

⁹N. A. Tahir, A. Adonin, C. Deutsch, V. E. Fortov, N. Grandjouan, B. Geil, V. Grayznov, D. H. H. Hoffmann, M. Kulish, I. V. Lomonosov, V. Mintsev, P. Ni, D. Nikolaev, A. R. Piriz, N. Shilkin, P. Spiller, A. Shutov, M. Temporal, V. Ternovoi, S. Udrea, and D. Varentsov, Nucl. Instrum. Methods Phys. Res. A **544**, 16 (2005).

¹⁰P. Renaudin, V. Recoules, P. Noiret, and J. Cl rouin, Phys. Rev. E **73**, 056403 (2006).

¹¹V. N. Korobenko and A. D. Rakhel, Phys. Rev. B **75**, 064208 (2007).

¹²J. Cl rouin, V. Recoules, S. Mazevet, P. Noiret, and P. Renaudin, Phys. Rev. B **76**, 064204 (2007).

¹³S. S. Yu, B. G. Logan, J. J. Barnard, F. M. Bieniosek, R. J.

- Briggs, R. H. Cohen, J. E. Coleman, R. C. Davidson, A. Friedman, E. P. Gilson, L. R. Grisham, D. P. Grote, E. Henestroza, I. D. Kaganovich, M. Kireeff Covo, R. A. Kishek, J. W. Kwan, E. P. Lee, M. A. Leitner, S. M. Lund, A. W. Molvik, C. L. Olson, H. Qin, P. K. Roy, A. Sefkow, P. A. Seidl, E. A. Startsev, J.-L. Vay, W. L. Waldron, and D. R. Welch, *Nucl. Fusion* **47**, 721 (2007).
- ¹⁴F. M. Bieniosek, J. J. Barnard, M. A. Leitner, A. W. Molvik, R. M. More, and P. K. Roy, *Nucl. Instrum. Methods Phys. Res. A* **577**, 284 (2007).
- ¹⁵J. Cl  rouin, P. Renaudin, and P. Noiret, *Phys. Rev. E* **77**, 026409 (2008).
- ¹⁶R. W. Lee, H. A. Baldis, R. C. Cauble, O. L. Landen, J. S. Wark, A. Ng, S. J. Rose, C. Lewis, D. Riley, J.-C. Gauthier, and P. Audebert, *Laser Part. Beams* **20**, 527 (2002).
- ¹⁷G. Pottlacher and H. J  ger, *J. Non-Cryst. Solids* **205-207**, 265 (1996).
- ¹⁸H. Hess, H. Schneidenbach, and Andres Kloss, *Phys. Chem. Liq.* **37**, 719 (1999).
- ¹⁹A. A. Likalter, *Physica A* **311**, 137 (2002).
- ²⁰L. Landau and J. Zeldovich, *Acta Physicochim URSS* **18**, 194 (1943).
- ²¹F. Hensel and W. W. Warren, *Fluid Metals* (Princeton University Press, Princeton, 1999).
- ²²A. Alavi, J. Kohanoff, M. Parrinello, and D. Frenkel, *Phys. Rev. Lett.* **73**, 2599 (1994).
- ²³D. Marx and J. Hutter, in *Modern Methods and Algorithms in Quantum Chemistry*, (NIC Series, Forschungszentrum Juelich, 2000), Vol. 1, p. 301.
- ²⁴The CPMD consortium at MPI f  r Festk  rperforschung and IBM Research Laboratory. See also <http://www.cpmid.org>
- ²⁵G. Faussurier, C. Blancard, and P. L. Silvestrelli, *Phys. Rev. B* **77**, 155126 (2008).
- ²⁶P. L. Silvestrelli, *Phys. Rev. B* **60**, 16382 (1999), and references therein.
- ²⁷N. F. Carnahan and K. E. Starling, *J. Chem. Phys.* **51**, 635 (1969).
- ²⁸J.-P. Hansen and I. R. McDonald, *Theory of Simple Liquids*, 2nd ed. (Academic, London, 1986).
- ²⁹N. W. Ashcroft and J. Lekner, *Phys. Rev.* **145**, 83 (1966).
- ³⁰N. W. Ashcroft and D. Stroud, *Solid State Phys.* **33**, 1 (1978).
- ³¹G. Faussurier and M. S. Murillo, *Phys. Rev. E* **67**, 046404 (2003).
- ³²C. Blancard and G. Faussurier, *Phys. Rev. E* **69**, 016409 (2004).
- ³³G. Faussurier, C. Blancard, P. Renaudin, and P. L. Silvestrelli, *Phys. Rev. B* **73**, 075106 (2006).
- ³⁴N. Troullier and J. L. Martins, *Phys. Rev. B* **43**, 1993 (1991).
- ³⁵P. E. Bl  chl and M. Parrinello, *Phys. Rev. B* **45**, 9413 (1992).
- ³⁶W. H. Press, S. A. Teukolski, W. T. Vetterling, and B. P. Flannery, *Numerical Recipes in Fortran: the art of scientific computing*, 2nd ed. (Cambridge University Press, New York, 1992).
- ³⁷L. Landau and E. Lifchitz, *Physique Statistique* (Editions Mir, Moscow, 1984).
- ³⁸M. Plischke and B. Bergersen, *Equilibrium Statistical Physics* (World Scientific, Singapore, 1994).
- ³⁹G. Parisi, *Statistical Field Theory* (Addison Wesley, Redwood City, 1988).
- ⁴⁰J. J. Binney, N. J. Dowrick, A. J. Fisher, and M. E. J. Newman, *The Theory of Critical Phenomena-An Introduction to the Renormalization Group* (Clarendon, Oxford, 1998).
- ⁴¹J. K. Johnson, J. A. Zollweg, and K. E. Gubbins, *Mol. Phys.* **78**, 591 (1993).
- ⁴²A. E. Mattsson, P. A. Schultz, M. P. Desjarlais, T. R. Mattsson, and K. Leung, *Modell. Simul. Mater. Sci. Eng.* **13**, R1 (2005).
- ⁴³D. A. Young and B. Alder, *Phys. Rev. A* **3**, 364 (1971).
- ⁴⁴A. A. Likalter, *Phys. Rev. B* **53**, 4386 (1996).
- ⁴⁵H. Hess, *Z. Metallkd.* **89**, 388 (1998).
- ⁴⁶J. K. Singh, J. Adhikari, and S. K. Kwak, *Fluid Phase Equilib.* **248**, 1 (2006).
- ⁴⁷A. Ray, M. K. Srivastava, G. Kondayya, and S. V. G. Menon, *Laser Part. Beams* **24**, 437 (2006).
- ⁴⁸I. V. Lomonosov, *Laser Part. Beams* **25**, 567 (2007).
- ⁴⁹S. Mazevet, L. A. Collins, N. H. Magee, J. D. Kress, and J. J. Keady, *Astron. Astrophys.* **405**, L5 (2003).
- ⁵⁰H. J. Monkhorst and J. D. Pack, *Phys. Rev. B* **13**, 5188 (1976).
- ⁵¹N. F. Mott, *Rev. Mod. Phys.* **40**, 677 (1968).
- ⁵²N. F. Mott, *Metal-Insulator Transition* (Taylor & Francis, London, 1974).
- ⁵³N. F. Mott, *Philos. Mag.* **6**, 287 (1961).
- ⁵⁴N. F. Mott, *Rep. Prog. Phys.* **47**, 909 (1984).
- ⁵⁵S. Mazevet, M. P. Desjarlais, L. A. Collins, J. D. Kress, and N. H. Magee, *Phys. Rev. E* **71**, 016409 (2005).
- ⁵⁶N. F. Mott, *Adv. Phys.* **16**, 49 (1967).
- ⁵⁷N. F. Mott, *Philos. Mag.* **26**, 1015 (1972).
- ⁵⁸N. F. Mott, *Philos. Mag.* **44**, 265 (1981).
- ⁵⁹A. F. Ioffe and A. R. Regel, *Prog. Semicond.* **4**, 237 (1960).
- ⁶⁰M. Gurvitch, *Phys. Rev. B* **24**, 7404 (1981).
- ⁶¹F. A. Chudnovskii, *J. Phys. C* **11**, L99 (1978).
- ⁶²S. Torquato, B. Lu, and J. Rubinstein, *Phys. Rev. A* **41**, 2059 (1990).
- ⁶³S.-H. Suh, W.-K. Min, V. Chihaiia, J.-W. Lee, and S.-C. Kim, *J. Korean Ind. Eng. Chem.* **17**, 351 (2000).
- ⁶⁴M. P. Desjarlais, J. D. Kress, and L. A. Collins, *Phys. Rev. E* **66**, 025401(R) (2002).
- ⁶⁵A. D. Rakhel, (private communication).
- ⁶⁶Ya. B. Zel'dovich and Yu. P. Raizer, *Physics of Shock Waves and High-Temperature Hydrodynamic Phenomena* (Dover, New York, 2002).